Domain Decomposition CN-FDTD with Unsplit-Field PML for Time-Reversed Channel Analysis

Xiao-Kun WEI, Wei SHAO, Xiao-Hua WANG, Bing-Zhong WANG

School of Physical Electronics, University of Electronic Science and Technology of China,
No. 4, Section 2, North Jianshe Road, 610054 Chengdu, China

weixiaokun1990@163.com, weishao@uestc.edu.cn, xhwang@uestc.edu.cn, bzwang@uestc.edu.cn

Submitted June 15, 2017 / Accepted December 5, 2017

Abstract. *In this paper, an efficient domain decomposition (DD) technique is introduced into the implicit Crank-Nicolson finite-difference time-domain (CN-FDTD) method to analyze the channel characteristics of time reversal (TR) waves. As an unconditionally stable time-marching method, DD-CN-FDTD is suitable to solve the multiscale problem involving special microstructures in a sub-wavelength array. The standard unsplit-field perfectly matched layer, which is implemented with auxiliary differential equations, is derived here to truncate the computational domain of a multipath indoor environment. Furthermore, each sub-matrix is preconditioned by the reverse Cuthill-Mckee scheme for easier lower-upper decomposition. Numerical results of TR wave propagation demonstrate the performance of the proposed method.*

Keywords

Domain decomposition (DD) technique, finite-difference time-domain (FDTD) method, perfectly matched layer (PML), time-reversal (TR)

1. Introduction

The finite-difference time-domain (FDTD) method has been widely used for solving electromagnetic problems, but its time step is constrained by the Courant-Friedrich-Levy (CFL) stability condition [1]. To remove this limit, the Crank-Nicolson (CN) scheme is introduced into FDTD to achieve unconditional stability [2], and it is more efficient than the conventional FDTD for solving multiscale problems. Recently, a domain decomposition (DD) technique has been introduced into weighted Laguerre polynomials (WLPs) based FDTD to get efficient solutions [3], [4].

The ultrawide-band (UWB) communication has gathered great interest due to its improved multiple-access capabilities and immunity to interference, but the communication quality will be decreased due to reflection, diffraction and scattering in a multipath propagation environment. Fortunately, the time reversal (TR) signal processing technique in [5] can make full use of multipath propagation created by various scatterers in an indoor environment [6]. In the TR scheme, the received power is concentrated at a specific time and location and very low co-channel interference in a multipath system can be achieved due to spatial and temporal focusing [7], [8]. For the numerical simulation of TR wave propagation, the number of unknowns is often large due to the fine structures and big computational range. Therefore, the generated large-scale sparse matrix in CN-FDTD leads to a heavy computational burden.

In this paper, the DD-CN-FDTD method is employed to simulate the multiscale electromagnetic problem of TR channel analysis in a two-dimensional (2-D) multipath indoor environment. The standard unsplit-field perfectly matched layer (PML) is derived for the absorbing boundary condition of DD-CN-FDTD with auxiliary differential equations (ADEs) [9]. Moreover, the reverse Cuthill-Mckee (RCM) technique [10] is employed to compress the bandwidth of sparse matrices and largely reduce the complexity of lower-upper (LU) decomposition. A numerical example of TR wave propagation is calculated to show the potential application of the proposed method.

2. Theory and Formulations

2.1 FDTD Method with the Crank-Nicolson Scheme

The time-domain Maxwell's equations for a 2-D transverse-electric (TE_z) wave propagating in free space can be written as

$$\varepsilon_0 \frac{\partial E_x\big|_{x,y,t}}{\partial t} = \frac{\partial H_z\big|_{x,y,t}}{\partial y} + J_x\big|_{x,y,t}, \tag{1a}$$

$$\varepsilon_0 \frac{\partial E_y\big|_{x,y,t}}{\partial t} = -\frac{\partial H_z\big|_{x,y,t}}{\partial x}, \tag{1b}$$

$$\mu_0 \frac{\partial H_z\big|_{x,y,t}}{\partial t} = \frac{\partial E_x\big|_{x,y,t}}{\partial y} - \frac{\partial E_y\big|_{x,y,t}}{\partial x} \tag{1c}$$

where ε_0 and μ_0 are the electric permittivity and magnetic permeability of free space, respectively.

Using the central difference scheme, we can transform the differential equations in (1) into difference ones. Then inserting (1c) into (1a) and (1b) with reference to [2], respectively, we can obtain the implicit updating equations for the electric field in CN-FDTD. Rewriting the implicit equations of E_x and E_y as a matrix form, we get

$$\boldsymbol{A}\boldsymbol{E}_{x,y}^{n+1} = \boldsymbol{b}^{n} + \boldsymbol{J}^{n+\frac{1}{2}}, \quad n = 0,1,2,\cdots \tag{2}$$

where $\boldsymbol{A}$ is the coefficient matrix, $\boldsymbol{E}_{x,y}$ is the unknown field vectors, $\boldsymbol{b}$ is the known terms and $\boldsymbol{J}$ is the current density.

2.2 Implementation of Domain Decomposition

In the DD structure, for example, the whole computational domain is decomposed into two subdomains, with the interface between the subdomains named as Γ_{1_2}, as shown in Fig. 1. For a specific simulated structure, a nonconformal DD scheme in which different sub-domains are discretized by different grids has been employed in the weighted Laguerre polynomial based FDTD [11]. The nonconformal DD scheme can also be implemented in CN-FDTD to handle the different grids on the interface between neighboring subdomains. Here, for simplicity, the graded nonuniform grids are used to divide the whole computational domain and the conformal domain interfaces are used.

The unknowns, namely the field components on the grids, are reordered by starting with the ones in D_1, followed by those in D_2, and ending with those associated with Γ_{1_2}. Then, the large matrix system (2) generated by the 2-D CN-FDTD method can be rewritten as [4]

$$\begin{pmatrix} \boldsymbol{A}_{11} & 0 & \boldsymbol{A}_{1\Gamma} \\ 0 & \boldsymbol{A}_{22} & \boldsymbol{A}_{2\Gamma} \\ \boldsymbol{A}_{\Gamma 1} & \boldsymbol{A}_{\Gamma 2} & \boldsymbol{A}_{\Gamma\Gamma} \end{pmatrix} \begin{pmatrix} \boldsymbol{E}_{x,y1} \\ \boldsymbol{E}_{x,y2} \\ \boldsymbol{E}_{x,y\Gamma} \end{pmatrix} = \begin{pmatrix} \boldsymbol{b}_1 \\ \boldsymbol{b}_2 \\ \boldsymbol{b}_\Gamma \end{pmatrix}. \tag{3}$$

Without loss of generality, it is assumed that the whole computational domain is decomposed into N subdomains. The matrix equation for the N-subdomain solution has the same form as (3). From (3), the linear system that is local to the ith subdomain (i = 1, 2, …, N) is written as

$$\boldsymbol{A}_{ii}\boldsymbol{E}_{x,yi} + \boldsymbol{A}_{i\Gamma}\boldsymbol{E}_{x,y\Gamma} = \boldsymbol{b}_i \tag{4}$$

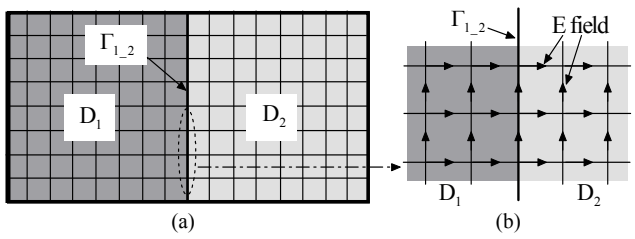

Fig. 1. (a) Two subdomains in a 2-D computational domain, (b) partitioning scheme.

and the linear system that is related to the interface can be written as

$$\sum_{i=1}^{N} \boldsymbol{A}_{\Gamma i}\boldsymbol{E}_{x,yi} + \boldsymbol{A}_{\Gamma\Gamma}\boldsymbol{E}_{x,y\Gamma} = \boldsymbol{b}_\Gamma . \tag{5}$$

From both (4) and (5), the variable $\boldsymbol{E}_{x,yi}$ can be eliminated from (5) and the Schur complement can be got

$$\boldsymbol{S}\boldsymbol{E}_{x,y\Gamma} = \boldsymbol{b}_\Gamma - \sum_{i=1}^{N} \boldsymbol{A}_{\Gamma i}\boldsymbol{A}_{ii}^{-1}\boldsymbol{b}_i \tag{6}$$

where $\boldsymbol{S} = \boldsymbol{A}_{\Gamma\Gamma} - \sum_{i=1}^{N} \boldsymbol{A}_{\Gamma i}\boldsymbol{A}_{ii}^{-1}\boldsymbol{A}_{i\Gamma}$ is the Schur complement.

Once the interface variables are obtained by solving the Schur complement system (6), (3) can be decoupled by solving the following subdomain problems

$$\boldsymbol{A}_{ii}\boldsymbol{E}_{x,yi} = \boldsymbol{b}_i - \boldsymbol{A}_{i\Gamma}\boldsymbol{E}_{x,y\Gamma}, \quad (i = 1,2,\cdots,N). \tag{7}$$

It is evident that the systems of (7) are independent of each other and can be solved in a parallel manner.

2.3 Formulations of Unsplit-Field PML

The frequency domain Maxwell's equations of a 2-D TE$_z$ wave in complex stretched coordinates can be written as [9]

$$\mathrm{j}\omega\varepsilon_0 E_x\big|_{x,y,\omega} = \frac{1}{S_y}\frac{\partial H_z\big|_{x,y,\omega}}{\partial y}, \tag{8a}$$

$$\mathrm{j}\omega\varepsilon_0 E_y\big|_{x,y,\omega} = -\frac{1}{S_x}\frac{\partial H_z\big|_{x,y,\omega}}{\partial x}, \tag{8b}$$

$$\mathrm{j}\omega\mu_0 H_z\big|_{x,y,\omega} = \frac{1}{S_y}\frac{\partial E_x\big|_{x,y,\omega}}{\partial y} - \frac{1}{S_x}\frac{\partial E_y\big|_{x,y,\omega}}{\partial x} \tag{8c}$$

where $\mathrm{j} = \sqrt{-1}$. And S_v (v = x, y) are the stretched coordinate matrix coefficients defined via the complex frequency shifted (CFS) PML parameters

$$S_v = \kappa_v + \frac{\sigma_v}{\alpha_v + \mathrm{j}\omega\varepsilon_0}, \quad v = x, y \tag{9}$$

where α_v, κ_v and σ_v are assumed to be positive real, and they are one-dimensional functions along the v-axis. Particularly, when $\alpha_v = 0$ and $\kappa_v = 1$, the standard unsplit-field PML can be derived for CN-FDTD.

To simplify the problem, but without loss of generality, the E_x component is taken as an example. With reference to [9], (8a) can be expressed as

$$\mathrm{j}\omega\varepsilon_0 E_x\big|_{x,y,\omega} = \frac{\partial H_z\big|_{x,y,\omega}}{\partial y} - \frac{\sigma_y}{\mathrm{j}\omega\varepsilon_0 + \sigma_y}\frac{\partial H_z\big|_{x,y,\omega}}{\partial y}. \tag{10}$$

The auxiliary variable is introduced into (10) as

$$Q_{y,z}^{H}\Big|_{x,y,\omega} = -\frac{\sigma_y}{\mathrm{j}\omega\varepsilon_0 + \sigma_y}\frac{\partial H_z\big|_{x,y,\omega}}{\partial y} \tag{11}$$

and then the expression of (10) can be directly transformed into a time-domain form

$$\varepsilon_0 \frac{\partial E_x\big|_{x,y,t}}{\partial t} = \frac{\partial H_z\big|_{x,y,t}}{\partial y} + Q_{y,z}^{H}\Big|_{x,y,t} \tag{12}$$

where the auxiliary variable $Q_{y,z}^{H}\big|_{x,y,t}$ satisfies the differential equation in time domain

$$\varepsilon_0 \frac{\partial Q_{y,z}^{H}\big|_{x,y,t}}{\partial t} + \sigma_y Q_{y,z}^{H}\Big|_{x,y,t} = -\sigma_y \frac{\partial H_z\big|_{x,y,t}}{\partial y}. \tag{13}$$

Similar to the derivation of (12) and (13), the time-domain expressions of other electromagnetic field components and auxiliary variables can also be obtained.

With reference to [2], the 2-D implicit E_x formulation of the standard unsplit-field PML for CN-FDTD can be given by using the central difference scheme to get the difference forms of (12) and (13). Inserting (13) and the difference equation of H_z into (12), the implicit updating equation for E_x can be got. Similarly, the updating equation of E_y can also be obtained.

2.4 Bandwidth Compression by RCM

Since the banded-sparse coefficient sub-matrices produced by DD-CN-FDTD keep unchanged during the time-marching process, the LU decomposition for each sub-matrix needs to be performed only once at the beginning of the calculation. The computational complexity of LU decomposition is $O(2m_1m_2n + m_2n - 2n)$, where n is the number of unknowns, m_1 is the bandwidth of the lower triangular matrix, and m_2 is the bandwidth of the upper one. The memory requirement of LU decomposition is $O(kn)$, where k is the bandwidth of the coefficient matrix [12]. In order to save calculation time and reduce memory requirement, the RCM technique [10] that generates a symmetric sparsity pattern with a small bandwidth is used for the coefficient matrices generated from the sub-domains.

3. Numerical Results

To validate the accuracy and efficiency of the proposed DD-CN-FDTD method for solving multiscale and electrically large electromagnetic problems, a numerical example of TR wave propagation is calculated in this section. In this section, a 2-D structure is analyzed for simplicity. However, the proposed method in this paper can be extended to solve three-dimensional scenarios. Here, all calculations are performed on an Intel (R) Core (TM) i3-2120×4 3.30 GHz machine with 12 GB RAM.

3.1 Channel Characteristics Extraction

To begin with, the channel characteristic of TR waves in a complicated multipath indoor environment is considered, as shown in Fig. 2. There are several fixed perfectly electric conductor (PEC) objects and one moving PEC object in the computational model. The box and chairs are dielectrics with ε_r = 1.5, and the walls are with ε_r = 4. A sub-wavelength array consists of the special microstructure of several metal sheets and it is loaded to the excitation source. The thickness of each sheet is 0.5 mm and its length is 400 mm.

To accurately model the geometry of the microstructure, the graded nonuniform grids along the y-axis are employed to divide the whole computational domain. The 2-D domain is 6 m × 4 m and is meshed into 300 × 280 rectangular grids, with the minimum cell size of 20 mm × 0.25 mm and the maximum one of 20 mm × 20 mm. The whole domain is terminated by 10 cells thick unsplit-field PML. The time variation of the source is given by

$$J_z(t) = \mathrm{e}^{-(t-t_0)^2/\tau^2}\sin\left[2\pi f_0(t-t_0)\right] \tag{14}$$

where f_0 = 0.65 GHz, f_{max} = 1 GHz, $\tau = 1/(2f_{max})$, and $t_0 = 3\tau$. The time step for FDTD is assigned to be Δt_{FDTD} = 0.4167 ps which satisfies the CFL condition, while the time steps for CN-FDTD and DD-CN-FDTD are $\Delta t_{CN\text{-}FDTD} = \Delta t_{DD\text{-}CN\text{-}FDTD} = 100\,\Delta t_{FDTD}$. In the DD structure, the computational domain is decomposed into four subdomains.

For the first procedure of TR simulation, the excitation is injected into H_z of the Source node. Conventional FDTD consists of 100 000 time steps, while both DD-CN-FDTD and CN-FDTD consist of 1 000 time steps, covering the same time interval. For the multiscale problems, it is computationally challenging for the conventional FDTD method due to the CFL stability limit. However, DD-CN-FDTD is an unconditionally stable scheme, and its time step is no longer restricted by the CFL stability limit. Thus, the much larger time step of DD-CN-FDTD results in the much smaller time-marching number. The UWB signal of H_z is recorded at Probe node. Then, the channel impulse response (CIR) of received UWB signal is extracted from the time-domain waveform by using the CLEAN algorithm presented in [13], as shown in Fig. 3. In a multipath indoor environment, the discrete impulse response $h(t)$ of the channel is modeled as a summation of reflected components. The real reflection response $y(t)$ to the input signal $s_{in}(t)$ can be computed by convolving $s_{in}(t)$ with $h(t)$. Then, $h(t)$ of a UWB channel can be extracted by deconvolving the reflection signal $y(t)$ from $s_{in}(t)$ with the CLEAN algorithm.

In the second procedure of TR simulation, the time-reversed waveform of the UWB signal, serving as the excitation function, is injected from the Probe node back

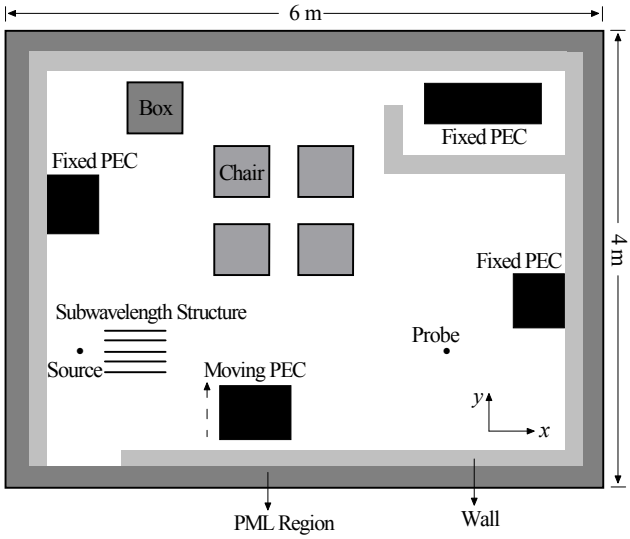

Fig. 2. Computational domain of a multipath indoor environment with the sub-wavelength array.

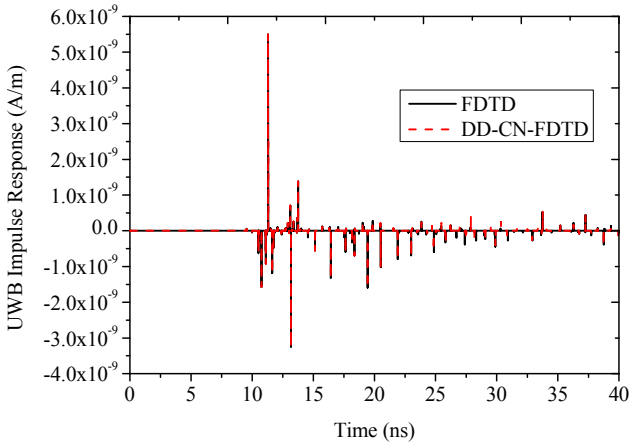

Fig. 3. CLEAN algorithm employed to extract impulse response from the received UWB signal.

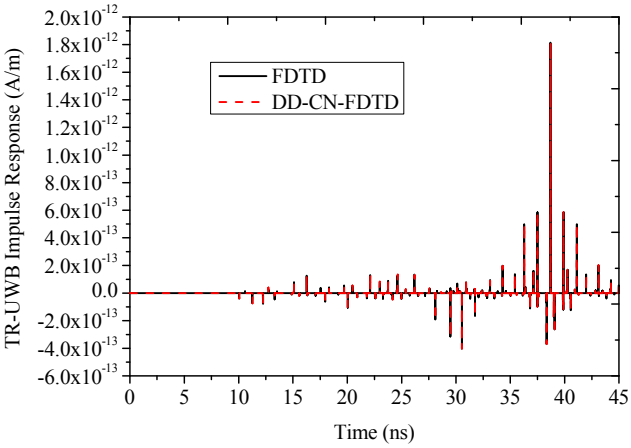

Fig. 4. CLEAN algorithm employed to extract impulse response from the received TR-UWB signal.

into the whole space. $N_t = 112\,000$ for FDTD while $N_t = 1\,120$ for DD-CN-FDTD and CN-FDTD are assigned. Here, the time-marching number should be larger than that in the first procedure to ensure the time-reversed waveform

Methods	δ_{UWB}	R_{UWB}
FDTD	4.3368	1.6773
CN-FDTD	4.3487	1.6966
DD-CN-FDTD	4.3348	1.6966

Tab. 1. Comparison among different methods for UWB channel.

Methods	$\delta_{TR\text{-}UWB}$	$R_{TR\text{-}UWB}$	C_{RMS}	G_{SNR}
FDTD	3.7601	3.0823	0.1330	1.8377
CN-FDTD	3.7407	3.0882	0.1398	1.8202
DD-CN-FDTD	3.7577	3.0870	0.1331	1.8195

Tab. 2. Comparison among different methods for TR-UWB channel.

Methods	Time step [ns]	Number of marching steps	CPU time [s]	Total memory [MB]
FDTD	0.4167	112 000	23274.58	28.85
CN-FDTD	41.6667	1 120	1613.24	2729.43
DD-CN-FDTD	41.6667	1 120	1294.95	1250.22

Tab. 3. Comparison of computer resources among different methods.

of the UWB signal recorded in the first procedure is totally injected into the whole space. The space-time focusing can be realized at the original Source node and the TR-UWB signal is recorded. The CIR of TR-UWB signal is also extracted by CLEAN, as shown in Fig. 4. From Figs. 3 and 4, the results from two methods are in good agreement.

To quantify the UWB and TR-UWB channels, several parameters of channel characteristics are defined to evaluate the performance of TR in wireless communication [14], [15]. A smaller root mean square (RMS) delay spread δ means reduced intersymbol interference (ISI) and improved communication quality, and a larger signal to noise ratio (SNR) R leads to better signal quality. Furthermore, the positive value of the temporal compression parameter C_{RMS} indicates that the RMS delay spread of the channel is reduced by TR. If the gain of signal to noise ratio G_{SNR} is larger than 1, the SNR of the channel is also improved by the TR technique. Table 1 shows the UWB channel characteristic parameters calculated from the three methods, and Table 2 shows the TR-UWB ones. It can be revealed from Tabs. 1 and 2 that the results from DD-CN-FDTD agree quite well with those from FDTD and CN-FDTD. As demonstrated in Tab. 2, C_{RMS} is positive and G_{SNR} is larger than 1, indicating that the TR technique reduces the ISI and improves the SNR due to its time-space focusing effect.

A comparison of computing resources among the three methods is shown in Tab. 3. DD-CN-FDTD results in a faster calculation with the pre-conditional RCM technique than the other two methods. Furthermore, the memory requirement of matrices $\boldsymbol{L}$ and $\boldsymbol{U}$ in DD-CN-FDTD is smaller than that in CN-FDTD.

3.2 Time-varying Communication System

The performance of the TR technique in a time-varying channel environment with fixed terminals (Source and Probe) and fixed objects is performed. A PEC bulk is mov-

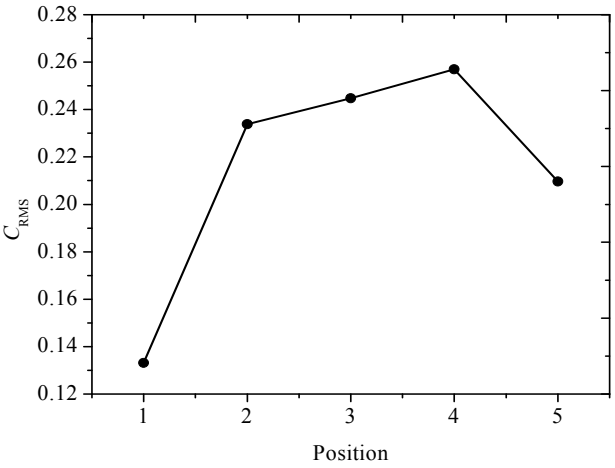

Fig. 5. C_{RMS} of the time-varying channel environment obtained from the DD-CN-FDTD method.

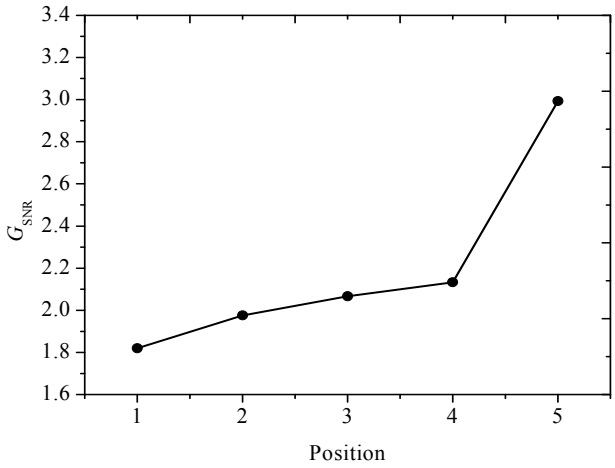

Fig. 6. G_{SNR} of the time-varying channel environment obtained from the DD-CN-FDTD method.

ing along the *y*-direction by 200 mm every time to realize a non-line-of-sight (NLOS) communication system. The channel parameters are evaluated when the moving PEC is placed at five different positions. Figures 5 and 6 illustrate C_{RMS} and G_{SNR} of the time-varying TR-UWB communication system as a function of position from the proposed method. It is shown in Figs. 5 and 6 that ISI is reduced and SNR is improved by the TR technique.

4. Conclusion

In this paper, the standard unsplit-field PML with ADEs is proposed for CN-FDTD and a DD technique is introduced to efficiently solve multiscale and electrically large TR problems. Compared with CN-FDTD, the small-scale sub-matrices in DD-CN-FDTD result in fast calculation and low memory requirement. The proposed method is used to calculate channel characteristic parameters of TR waves in a multipath indoor environment, and the results demonstrate its accuracy and efficiency.

Acknowledgments

This work was supported in part by the National Natural Science Foundation of China under Grant 61471105 and Grant 61331007 and in part by the 973 Project (No. 613273).

References

[1] TAFLOVE, A., HAGNESS, S. C. *Computational Electromagnetics: The Finite-Difference Time-Domain Method*. Norwood, MA, USA: Artech House, 2005. ISBN: 1580538320

[2] SUN, G., TRUEMAN, C. W. Approximate Crank-Nicolson schemes for the 2-D finite-difference time-domain method for TEz waves. *IEEE Transactions on Antennas and Propagation*, 2004, vol. 52, no. 11, p. 2963–2972. DOI: 10.1109/TAP.2004.835142

[3] WEI, X. K., SHAO, W., SHI, S. B., WANG, B. Z. An efficient 2-D WLP-FDTD method utilizing vertex-based domain decomposition scheme. *IEEE Microwave and Wireless Component Letters*, 2015, vol. 25, no. 12, p. 769–771. DOI: 10.1109/LMWC.2015.2495210

[4] WEI, X. K., SHAO, W., SHI, S. B., CHENG, Y. F., WANG, B. Z. An optimized higher order PML in domain decomposition WLP-FDTD method for time reversal analysis. *IEEE Transactions on Antennas and Propagation*, 2016, vol. 64, no. 10, p. 4374–4383. DOI: 10.1109/TAP.2016.2596899

[5] FINK, M. Time reversal of ultrasonic fields—part I: basic principles. *IEEE Transactions on Ultrasonics, Ferroelectrics, and Frequency Control*, 1992, vol. 39, no. 5, p. 555–566. DOI: 10.1109/58.156174

[6] ZHOU, C. M., GUO, N., QIU, R. C. Time-reversed ultra-wideband (UWB) multiple input multiple output (MIMO) based on measured spatial channels. *IEEE Transactions on Vehicular Technology*, 2009, vol. 58, no. 6, p. 2884–2898. DOI: 10.1109/TVT.2008.2012109

[7] KHALEGHI, A. Measurement and analysis of ultra-wideband time reversal for indoor propagation channels. *Wireless Personal Communications*, 2010, vol. 54, no. 5, p. 307–320. DOI: 10.1007/s11277-009-9727-y

[8] WEI, X. K., SHAO, W., OU, H., WANG, B. Z. Efficient WLP-FDTD with complex frequency-shifted PML for super-resolution analysis. *IEEE Antennas and Wireless Propagation Letters*, 2017, vol. 16, p. 1007–1010. DOI: 10.1109/LAWP.2016.2616289

[9] GEDNEY, S. D., ZHAO, B. An auxiliary differential equation formulation for the complex-frequency shifted PML. *IEEE Transactions on Antennas and Propagation*, 2010, vol. 58, no. 3, p. 838–847. DOI: 10.1109/TAP.2009.2037765

[10] CUTHILL, E., MCKEE, J. Reducing the bandwidth of sparse symmetric matrices. In *Proceedings of the 1969 24th National Conference on ACM*. New York (USA), 1969, p. 157–172. DOI: 10.1145/800195.805928

[11] YI, M., QIAN, Z. G., AYDINER, A., SWAMINATHAN, M. Transient simulation of multiscale structures using the nonconformal domain decomposition Laguerre-FDTD method. *IEEE Transactions on Components, Packaging and Manufacturing Technology*, 2015, vol. 05, no. 4, p. 532–540. DOI: 10.1109/TCPMT.2015.2411744

[12] GOLUB, G. H., VAN LOAN, C. F. *Matrix Computations*. 4th ed., USA: Johns Hopkins University, 2014. ISBN: 97814214079 44

[13] BUCCELLA, C. FELIZIANI, M., MANZI, G. Detection and localization of defects in shielded cables by time-domain measurements with UWB pulse injection and clean algorithm post processing. *IEEE Transactions on Electromagnetic Compatibility*, 2004, vol. 46, no. 4, p. 597–605. DOI: 10.1109/TEMC.2004.8378 42

[14] NAQVI, I. H., BESNIER, P., ZEIN, G. E. Robustness of a time-reversal ultra-wideband system in non-stationary channel environments. *IET Microwaves, Antennas and Propagation*, 2011, vol. 5, no. 4, p. 468–475. DOI: 10.1049/iet-map.2010.0127

[15] WEI, X. K., SHAO, W., OU, H., WANG, B. Z. An efficient higher-order PML in WLP-FDTD method for time reversed wave simulation. *Journal of Computational Physics*, 2016, vol. 321, no. 9, p. 1206–1216. DOI: 10.1016/j.jcp.2016.06.032

About the Authors …

Xiao-Kun WEI was born in Tianshui, Gansu Province, China, in 1990. He received the B.S. degree in Electronic Information Science and Technology and M.S. degree in Electronics and Communication Engineering from the University of Electronic Science and Technology of China (UESTC), Chengdu, China, in 2013 and 2015, respectively. Now, he is working toward the Ph.D. degree in Radio Physics at UESTC. From 2016 to 2017, he was an International Visiting Graduate Student in the Dept. of Electrical and Computer Engineering, University of Toronto, Toronto, ON, Canada. His research interests are unconditionally stable time-domain numerical methods and optimization techniques in electromagnetics.

Wei SHAO (corresponding author) was born in Chengdu, China, in 1975. He received the B.E. degree in Electrical Engineering from UESTC in 1998, and received M.Sc. and Ph.D. degrees in Radio Physics from UESTC in 2004 and 2006, respectively. He joined the UESTC in 2007 and is now a Professor there. From 2010 to 2011, he was a Visiting Scholar in the Electromagnetic Communication Laboratory, Pennsylvania State University, State College, PA. From 2012 to 2013, he was a Visiting Scholar in the Dept. of Electrical and Electronic Engineering, Hong Kong University. His research interests include computational electromagnetics and antenna design.

Xiao-Hua WANG was born in Jiangsu Province, China, in 1980. He received the B.S. degree in Electrical Engineering, M.S. and Ph.D. degrees in Radio Physics from the University of Electronic Science and Technology of China (UESTC), Chengdu, China, in 2002, 2005, and 2008, respectively. From Mar. 2008 to Feb. 2009, he was an RF Research Engineer with Huawei Company, Shenzhen, China. From Mar. 2009 to Feb. 2010, he was with the Department of Electronic Engineering, City University of Hong Kong, Kowloon Tong, Hong Kong, as a Research Staff. Currently, he is an Associate Professor with UESTC. His research interests include computational electromagnetics, microwave passive circuits, and antenna design.

Bing-Zhong WANG received the Ph.D. degree in Electrical Engineering from UESTC, Chengdu, China, in 1988. He joined the UESTC in 1984 where he is currently a Professor. He has been a Visiting Scholar at the University of Wisconsin-Milwaukee, a Research Fellow at the City University of Hong Kong, and a Visiting Professor in the Electromagnetic Communication Laboratory, Pennsylvania State University, State College, PA. His current research interests are in the areas of computational electromagnetics, antenna theory and technique, and electromagnetic compatibility analysis.